Available online at www.sciencedirect.com
SCIENCE DIRECT®
ELSEVIER
Journal of the European Ceramic Society xxx (2006) xxx–xxx
ECERS
www.elsevier.com/locate/jeurceramsoc

Copper and silver nanocrystals in lustre lead glazes: Development and optical properties

J. Roqué [a,*], J. Molera [b], P. Sciau [c], E. Pantos [d], M. Vendrell-Saz [a]

[a] *Departament de Cristal·lografia Mineralogia i Dipòsits minerals, Universitat de Barcelona, 08028 Barcelona, Spain*
[b] *Deptartament de Física, Universitat de Girona, 17071 Girona, Spain*
[c] *CEMES/CNRS, BP 94347 31055 Toulouse Cedex 4, France*
[d] *CCLRC Synchrotron Radiation Source/Daresbury Laboratory, Warrington WA4 4AD, UK*

Received 21 September 2005; received in revised form 9 December 2005; accepted 16 December 2005

Abstract

In the early 9th century AD ancient potters of Iraq discovered that after firing some copper oxides and silver salts with clay, iron oxides and some sulphur compounds applied on a ceramic glaze produced a beautiful layer with a wide range of colours, from reddish to yellowish or even greenish, and some with a characteristic metallic copper or purplish shine. Modern studies of these layers showed that they are formed by nanocrystals of copper and silver embedded in a glass matrix. Some attempts have been performed to understand ancient lustre coloration and characteristic gloss but have failed to give a clear correlation between chemical composition and colour, and generally make some assumptions on the shape and the size of the nanoparticles and the lustre nanostructure. The aim of this paper is to establish a basis for understanding lustre nanostructure linked to its optical properties from a sequence of lustre reproductions on traditional lead glazed tiles. These modern lustre decorations have been studied by means of optical microscopy, transmission electron microscopy and electron energy loss spectroscopy, UV–vis spectroscopy, low irradiation angle X-ray diffraction, synchrotron radiation X-ray diffraction and electron microprobe analysis. These results show that changes in the lustre nanostructure affect the glaze colour and shine during the lustre formation process. Lustre nanostructure showed crystal size range as a function of depth, that subsequently disappeared followed by an increase of nanoparticles mean diameter and reduction of the interparticle distances. Consequently, the dipole plasmon coupling between copper nanoparticles appeared, and seems to be responsible for the metallic shine and copper metal like coloration of the copper lustre. However, colour from the glaze surface differs when calculated for diffuse or reflected light. Diffuse coloration appears strongly affected by the copper nanocrystals, while specular coloration is not only affected by copper but also by the presence of an inhomogeneous distribution of silver nanocrystals which gives the lustre a characteristic purplish shine.

Keywords: Firing; Nanocomposite; Optical properties; Glass ceramics

1. Introduction

Lustre is one of the most interesting medieval ceramic decorations that corresponds to a nanostructured thin layer formed by metallic copper and silver nanocrystals embedded in a glass matrix.[1–4] The earliest lustres were probably made in Iraq in the early 9th AD and followed the expansion of the Arabian culture through Spain and the rest of the western Mediterranean.[5–7] Ancient craftsmen, and still nowadays in some places of Spain, obtained lustre by applying a copper and silver containing paint, mixed with water and/or vinegar, on a glazed ceramic, which afterwards, was annealed in a reducing atmosphere. Inside the kiln, the raw paint reacted with the glaze surface, and after firing, the remaining paint was washed off revealing the lustre decoration beneath.[7,8] Hence, traditional lustre technique is one of the oldest technologies known to achieve metal-glass nanocomposites under relatively controlled conditions, without the need of ultra high vacuum or clean environments.

Recently, it has been demonstrated that the lustre formation process takes place as a result of an ionic exchange process.[8–11] Nowadays, several methods have been reported for the synthesis of nanosized particles of ceramic materials; among them the ion-exchange process has also been widely used to dope alkali silicate glasses. Ion-exchange in glass is typically carried out

* Corresponding author. Tel.: +34 934021357; fax: +34 934021340.
E-mail address: josep.roque@ub.edu (J. Roqué).

0955-2219/$ – see front matter © 2006 Elsevier Ltd. All rights reserved.
doi:10.1016/j.jeurceramsoc.2005.12.024

by replacing monovalent alkali ions present in a surface layer of a glass substrate with different ions, usually from a molten salt bath.[12] Traditional lustre technology is based in the same ion-exchange process but instead of using a salt bath, the ion-exchange takes place between the copper and silver containing raw paint (traditionally called cosela) and the lead alkali glaze.[10]

Lustre required deep knowledge from the artisans of the raw materials used and on the kiln conditions, and their empirical knowledge led to the achievement of colourful lustre decorations with a wide range of colours, from reddish to yellowish or even greenish, and some with a characteristic metallic or purplish shine. But how were the optical glaze properties modified by nanoparticles in order to fulfil these aesthetic purposes? Some attempts have been performed to understand ancient lustre coloration but hardly give a clear correlation between chemical composition and lustre colour,[13,14] and generally make some assumptions regarding nanoparticles shape, size and lustre nanostructure. Hence, the aim of this paper is to establish a basis for understanding copper lustre nanostructure linked to its colour and characteristic shine.

The process of lustre development is studied using a sequence of traditional lead glazed traditional tiles, samples R1, R2, R3 and R4, obtained by extraction from the kiln at intervals of time during the last 20 min of lustre firing. These samples are successive steps of production and only the two last ones showed a characteristic fully developed metallic shine lustre decoration. These modern lustre decorations have been studied by means of reflectance optical microscopy (OM) in dark and bright field modes as a first approach; by transmission electron microscopy and electron energy loss spectroscopy (TEM-EELS) to observe lustre nanostructure and nanoparticles chemical composition; by means of UV-spectroscopy to acquire the reflectance and absorption spectra of lustre in the visible range; by synchrotron radiation X-ray diffraction (SR-XRD) to determine the crystalline phases present; and by electron microprobe analysis (EMPA) to get the overall chemical compostion of lustre decorations through the lustre formation process.

2. Characterization of lustre decoration layers

2.1. Obtaining samples

Modern lustre ceramic reproduction was obtained following the traditional techniques still alive in the region of València (Spain).[8] The lustre raw powder was mixed with water and applied by brush over an already fired lead glaze tile (5 cm × 5 cm). The lustre raw powder contains 12 wt.% quartz (SiO_2), 43 wt.% illite, 10 wt.% calcite $CaCO_3$), 15 wt.% iron oxides (Fe_2O_3), 7 wt.% gypsum $CaSO_4{\cdot}2H_2O$) and 13 wt.% tenorite (CuO) and some traces of silver (0.15 wt.% of Ag_2O). The lustre raw powder was allowed to dry before firing. Lustre tiles were annealed in a typical two chamber (100 cm × 100 cm) kiln, at temperatures of about 550 °C during 20 min in a more or less reducing atmosphere produced by burning rosemary.[8] Tile samples (R1–R4) were extracted sequentially at the maximum temperature and water quenched, and correspond to a sequence from early to full lustre development as seen on Fig. 1. The

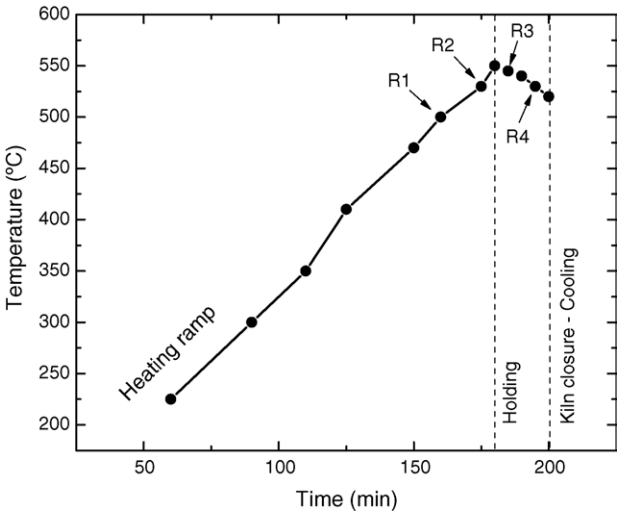

Fig. 1. Relation between temperatures and time during samples extraction from the traditional kiln. Samples were extracted in the temperature range 500–550 °C, when the traditional kiln reached the maximum of the heating ramp.

remain of the lustre raw powder was washed off after firing, revealing the lustre decoration beneath.

2.2. Reflectance and absorbance UV–vis spectra acquisition on lustre decoration layers

OM in reflectance mode gives the first insights of the optical properties of lustre decoration and how the lustre formation process modifies the main glaze optical properties. When the polarized light strikes the glaze surface, the overall reflectance collected by the objective is called reflectance with the specular component included (RSCI). RSCI can be considered as the reflectance resulting from two components, namely the reflectance of the specular component (RSC) or specular reflectance and the reflectance with the specular component excluded (RSCE) or diffuse reflectance. The RSC corresponds to a certain proportion of the incident light that is reflected directly from the surface at the opposite angle to the incident light, while the RSCE corresponds to the proportion of light that penetrates into the glaze and is scattered. When light strikes the glaze surface, the RSCI is what the observer sees, but the evolution of this RSCI through samples R1, R2, R3 and R4 is determined by the evolution and/or enhancement of RSC and/or RSCE due to the lustre formation.

Reflectance UV–vis spectra have been recorded using a portable spectrophotometer model Minolta CM-2600d equipped with a 52 mm barium sulphate integrating sphere, dual beam geometry, 360–740 nm wavelength range with 10 nm measurement intervals of 3 s irradiating a 3 mm diameter area. The reflectance with the specular component included (RSCI) and the reflectance with the specular component excluded (RSCE) spectra were acquired simultaneously. In order to obtain the spectrum of reflectance of the specular component (RSC), RSCE was subtracted from RSCI. From the dispersion of both reflectances, colour coordinates and attributes (including domi-

nant wavelength λ_D, which corresponds to the hue) were calculated according to the International Commission on Illumination (usually known as the CIE).

Additionally, absorption spectra in the UV–vis range have been also measured on thin sections of samples R1–R4 by means of spectrophotometer Shimadzu UV-2101 PC within the range 360–800 nm, with an interval of measurement of 0.5 nm, with a 0.5 mm beam footprint and at medium speed of measurement. The absorption band resulting from the dipole plasmon resonance on metallic nanoparticles was expected to be measured.

2.3. Determining lustre chemical composition and nanostructure

Chemical analyses and distribution mappings of Cu and Ag, from the lustre layers were performed by microprobe analysis (EPMA Cameca SX-50) and the measurement conditions were 20 kV and 15 nA probe current and 2 nA probe current for Na with a measurement spot size of about 5 μm. Analyses were performed directly on the surface of the samples. The penetration depth was evaluated by Kanaya Okayama Range,[15] giving about 2.5 μm in the glaze, and 1 μm in a lustre layer, assumed to be formed by 50% glaze and 50% metal. The penetration depth is greater than the thickness of the lustre layer and the measurements give an average value over the whole analyzed depth.

TEM Philips CM20 coupled with DIGIPEELS 666 permitted the characterization the nanostructure, nanoparticle shape, sizes and chemical composition. With TEM-EELS, it is possible to establish the evolution of the nanoparticles inside the glass matrix through samples R1, R2, R3 and R4. In order to perform TEM-EELS observations, glaze cross-sections from each sample were prepared, polished mechanically and thinned by means of Ar^+ ion bombardment to achieve the appropriate thickness to allow electrons pass through the sample (around 100 nm). To perform chemical elemental analysis of the nanoparticles electron energy loss spectrums (EELS) were acquired.

Crystalline phases were identified and studied by XRD using a Siemens D-500 equipped with a secondary monochromator and Cu tube (wavelength 1.5418 Å). According to the nanostructured thin layer nature of lustre, low irradiation angle XRD measurements (2.0 s counting time and 0.05 2θ step) were performed to determine the crystalline phases present. To estimate the mean size of the copper metal nanoparticles on the lustre, thin slides of the glazes were prepared and examined by X-ray diffraction in transmission geometry at station 9.6 of the synchrotron radiation source (SRS) at Daresbury Laboratory. These sections were thin enough to allow the X-rays to pass through the glass and diffract. The wavelength at station 9.6 was 0.87 Å and the collimator defining the beam footprint had a cross-section of 200 μm. The data collection time was typically 60 s using an ADSC Quantum-4 CCD detector at a distance of 160 mm. The active area of the detector is 2304 × 2304 pixels. The pixel size is 81.6 μm × 81.6 μm and the dynamical range 16-bit. The data were processed using the ESRF package FIT2D.[16]

3. Optical properties and copper/silver nanoparticles thin layer development in lustre decorations

3.1. Reflectance and absorbance in the UV–vis range

At first sight, from these modern lustre reproductions two subsets of samples can be observed, according to colour and reflectance: Samples R1 and R2 do not present a metallic shine although they are coloured light orange while samples R3 and R4 exhibit a metallic and purplish shine and have a metallic copper-like colouration.

In Fig. 2, OM in reflectance mode images are shown. Images from samples R1 and R2 show small yellowish-orange bright spots with sizes up to 5 μm, with a higher density in sample R2 than in R1. Samples R3 and R4 both show a fully developed lustre with a nice gold metallic shine. R3 shows a higher reflectance at the edges than at the centre of the lustre decorations. The edges appear bright orange and contain some highly reflecting yellowish-orange spots; the centre shows a lower reflectance and orange-yellow colour. R4 exhibits a highly reflecting gold-like edge and also an orange-yellow colour. It is interesting to notice the presence of scattered blue spots on samples R3 and R4 that correspond to accumulations of metallic silver particles.[4]

The RSCE and RSC spectra acquired in the 360–800 nm wavelength range from the lustre decoration surfaces show a clear evolution from sample R1 to sample R4 as seen in Fig. 3. The RSCE spectra for sample R1 correspond to a lead glaze with a strong absorption in the blue region,[17] while for samples R2, R3 and R4, the overall absorption increase and the absorption in the blue region is much less pronounced than in sample R1. Moreover, a small absorption band appears around 560 nm and increases from sample R2 to sample R4. During the lustre formation, the reflectance on the red region of the RSCE spectra increases through samples R2, R3 and R4, linked to the presence and development of the lustre decoration layer.

The RSC spectra show an increase of intensity from sample R1 to R4 as seen in Fig. 3. According to the intensity of RSC, two sets of samples can be established: Samples R1 and R2 with a very low or non-existent RSC, and samples R3 and R4 with a higher RSC. In samples R3 and R4, the RSC show a strong reflectance in the red region, and surprisingly also reflects in the blue region. Two absorption bands appear in the RSC spectra from samples R3 and R4, one around 560 nm and a second one around 430 nm, with a strong increase in the 560 nm absorption band from sample R3 to R4.

Dominant wavelength λ_D values have been calculated from the RSC and RSCE spectra for each sample and are listed in Table 1. The calculated colour from the RSC show an evolution from λ_D 582 nm and 0.21% excitation purity on sample R1 to λ_D 602 nm 0.32% excitation purity in sample R4, and the calculated colour from the RSCE showed an evolution from λ_D 475 nm and 0.07% excitation purity on sample R1 to λ_D 585 nm 0.19% excitation purity on sample R4. These results confirm that colouration of lustre evolves towards more reddish values from the very beginning until the end of the lustre formation process.

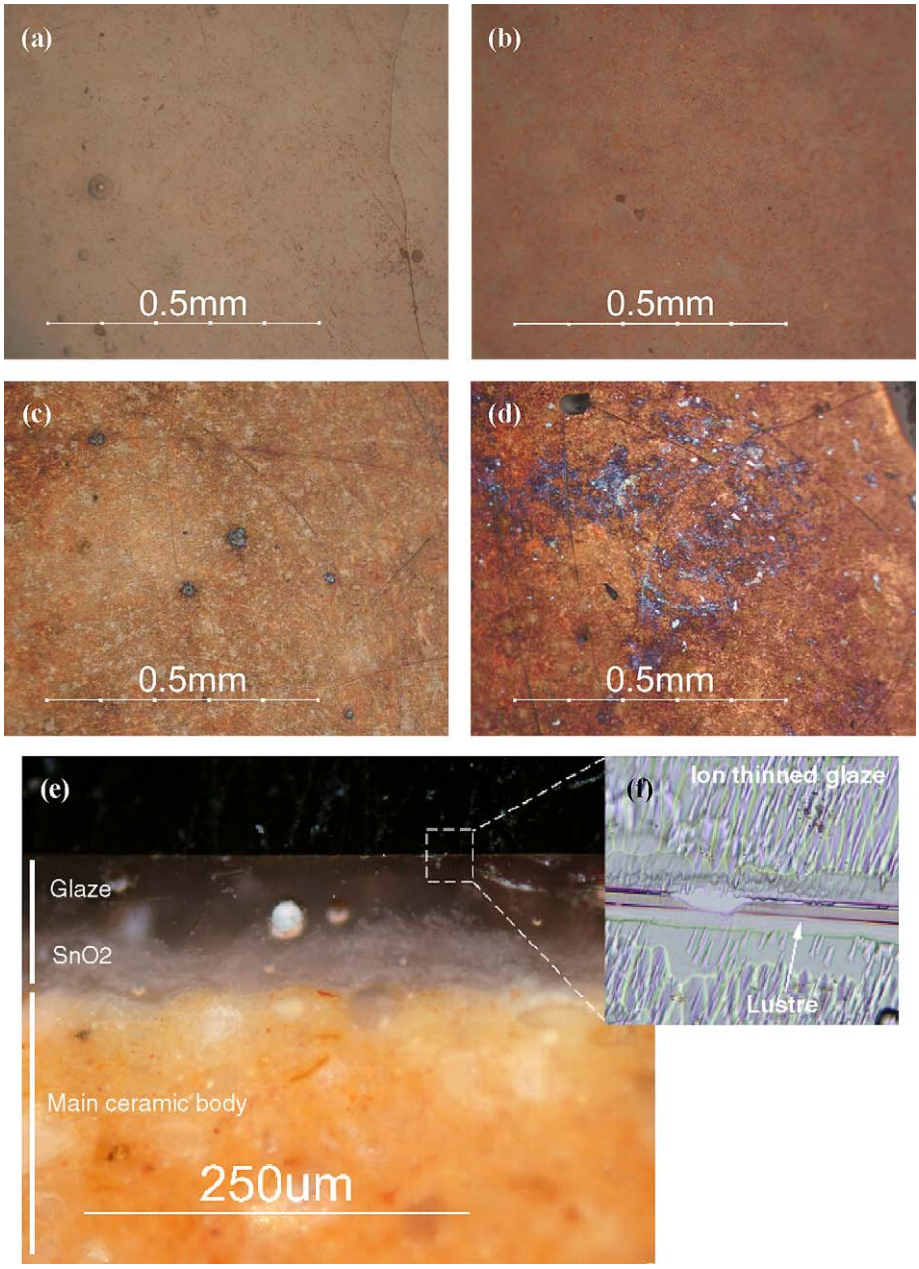

Fig. 2. OM images from lustre surfaces decorations and glaze cross sections (a) Sample R1 showing the lead glaze surface; (b) sample R2, the glaze starts to be concealed by the lustre and scattered yellowish-orange spots appear; (c) sample R3 showing the lustre decoration with a strong yellowish-orange reflectance and bluish spots corresponding to silver nanocrystals aggregates; (d) sample R4, the bulk glaze is completely concealed and has a strong yellowish-orange reflectance. Scattered bluish spots related to silver can be also seen; (e) cross-section micrograph obtained by means of reflection OM in dark field from sample R4 showing the cassiterite layer in-depth the glaze at the top of the main ceramic body; (f) OM cross section micrograph obtained in transmission mode in bright field from the ion-thinned glaze during TEM sample preparation showing a red line at the glaze surface corresponding to the lustre decoration layer. (For interpretation of the references to color in this figure legend, the reader is referred to the web version of this article.)

Table 1
Mean nanocrystals diameter obtained by SR-XRD and copper plasmon absorption band position and width and the correlation coefficient resulting from Gaussian fitting

Sample	λ_D RSCE (nm)	Purity (%)	CIE colour	λ_D RSC (nm)	Purity (%)	CIE colour	Shine
R1	475	0.07	Blue	582	0.21	Yellowish orange	Non-metallic
R2	583	0.1	Yellowish orange	586	0.15	Yellowish orange	Non-metallic
R3	582	0.14	Yellowish orange	589	0.65	Orange	Metallic/purplish
R4	585	0.19	Yellowish orange	602	0.32	Reddish orange	Metallic/purplish

The plasmon absorption band shifts towards reddish positions and becomes wider.

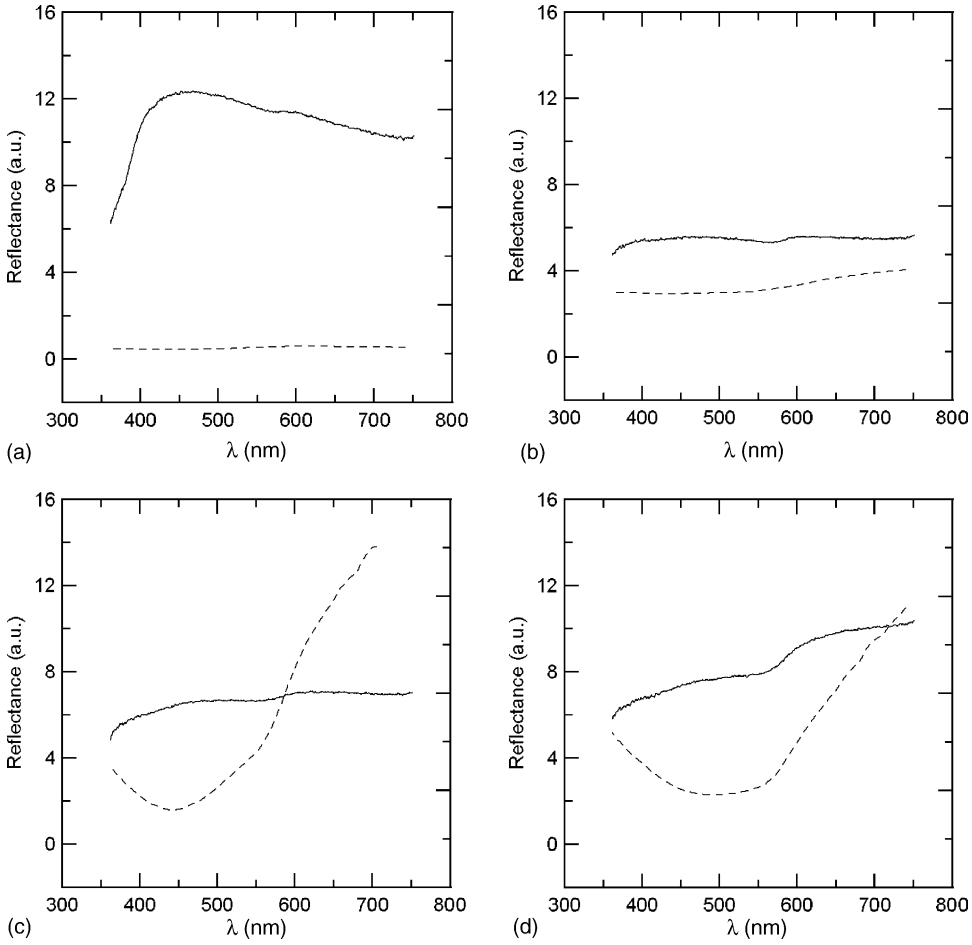

Fig. 3. RSCE and RSC spectra on lustre reproductions: (a) sample R1 with a RSCE corresponding to a lead glaze with a strong absorption at the beginning of the blue region and almost no RSC; (b) sample R2, the lustre layer conceals the glaze increasing its RSCE in the red region and very low RSC appears; (c) sample R3 increase its RSCE in the red region and RSC is strongly enhanced; (d) sample R4, the RSCE also increase its reflectance on the red region and RSC is strongly enhanced.

From the absorption spectra acquired in the 360–800 nm wavelength range from thin sections using transmission geometry and shown in Fig. 4, two main absorption bands appear in Fig. 4(a): one in the blue region, constant in all the samples and related to the absorption of the lead glaze substrate, and a second one at 560 nm corresponding to the dipolar plasmon absorption of metallic copper nanoparticles,[18] which only occurs on samples R2, R3 and R4. The absorption band at 560 nm has been Gaussian fitted and the results are listed in Table 2. They show a red shift from 567 nm in sample R2 to 577 nm in sample R3 and 585 nm in sample R4. Normalized spectra in Fig. 4(b) from samples R2, R3 and R4 confirm this red shift and show an increase of the absorption in the red region resulting from an increase on the right shoulder of the absorption band. This absorption becomes more important from sample R3 to sample R4.

Table 2
Dominant wavelength (λ_D) from RSCE and RSC spectra acquired on samples R1, R2, R3 and R4

Sample	Mean Cu nanorystals diameter (nm)	SPR (nm)	FHW (nm)	Correlation coefficient R^2
R1	–	–	–	–
R2	9.29 ± 1.91	567	41.61	0.99953
R3	9.14 ± 0.88	577	48.66	0.99978
R4	21.95 ± 0.77	585	49.02	0.99977

3.2. Chemical composition and copper/silver distribution

EPMA chemical profiles were acquired directly on the surface of the samples crossing white glaze and lustre decoration and the mean composition has been calculated and listed in Table 3. Chemical differences are seen on the lustre from the early formation stage of lustre, sample R1, to the full lustre formation on sample R4. An increase of copper and silver concentration, from 0.22 ± 0.13 to 5.32 ± 0.75 wt.% and from 0.03 ± 0.04 to 0.98 ± 0.30 wt.%, respectively, and a decrease on sodium and potassium concentration, from 0.70 ± 0.06 to 0.50 ± 0.04 wt.% and from 3.43 ± 0.28 to 1.99 ± 0.12 wt.%, respectively, is observed during the lustre formation process. Copper increases rapidly at the beginning of the lustre formation process (from 0.2 ± 0.1 wt.% on sample R1 to 4.0 ± 0.6 wt.% on sample R2) while later silver increases suddenly (from 0.05 ± 0.05 wt.% on sample R2 to 1.0 ± 0.4 wt.% on sample

Table 3
Elemental composition of glazes obtained from EMPA data taken on the lustre glazes surfaces in wt.% for samples R1, R2, R3 and R4

Sample	Na	K	Mg	Al	Si	Ca	Fe	Cu	Ag	Pb	O	Total
R1	0.70 ± 0.06	3.43 ± 0.28	0.04 ± 0.03	2.67 ± 0.10	21.77 ± 0.15	0.75 ± 0.19	0.06 ± 0.05	0.22 ± 0.13	0.03 ± 0.04	36.35 ± 0.78	31.34 ± 0.17	97.37 ± 1.98
R2	0.69 ± 0.06	3.32 ± 0.36	0.06 ± 0.02	2.88 ± 0.07	21.97 ± 0.25	0.85 ± 0.09	0.08 ± 0.08	1.31 ± 0.54	0.05 ± 0.05	34.62 ± 0.58	32.84 ± 0.24	96.67 ± 2.34
R3	0.56 ± 0.05	1.98 ± 0.10	0.03 ± 0.02	2.52 ± 0.07	21.03 ± 0.17	0.66 ± 0.07	0.07 ± 0.04	3.98 ± 0.58	1.02 ± 0.38	35.10 ± 0.74	30.90 ± 0.18	97.84 ± 2.4
R4	0.50 ± 0.04	1.99 ± 0.12	0.04 ± 0.01	2.15 ± 0.05	20.69 ± 0.17	0.73 ± 0.05	0.07 ± 0.04	5.32 ± 0.75	0.98 ± 0.30	34.40 ± 0.66	31.03 ± 0.18	97.90 ± 2.37

An increase in copper and silver and a decrease in sodium and potassium are seen through the lustre formation process.

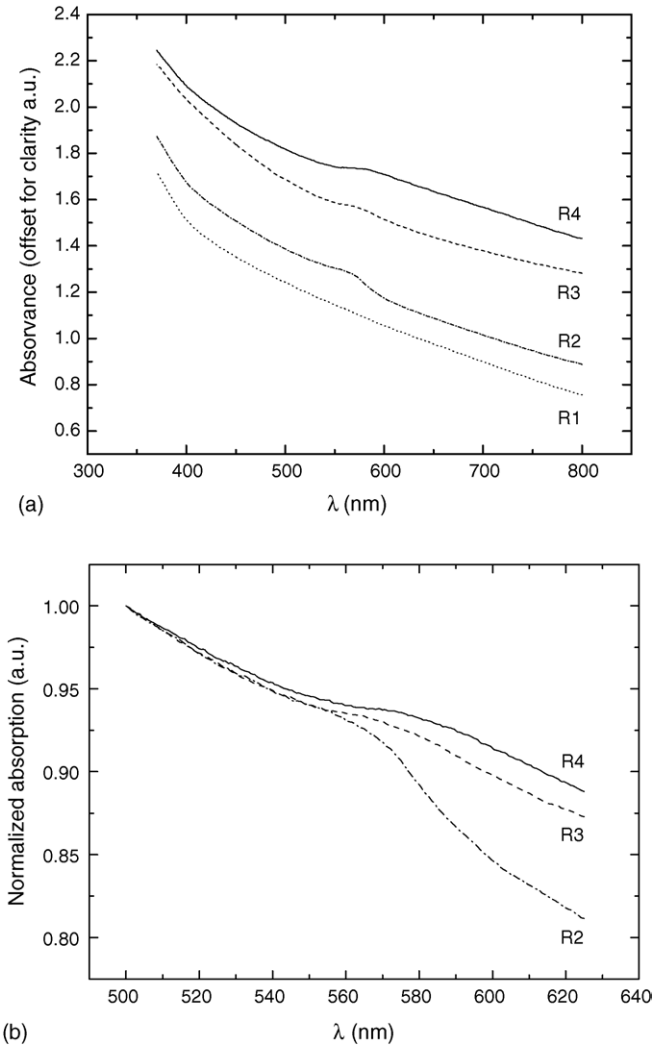

Fig. 4. Absorption spectra obtained from lustre reproductions R1, R2, R3 and R4. (a) Strong absorption at the beginning of the blue region due to the lead glaze and copper dipole plasmon absortion band. (b) Copper dipole plasmon absorption band shift in position and width as a consequence of dipole interactions between nanoparticles through samples R1, R2 and R3.

R3). This has been interpreted as a result of the chemical mechanisms responsible for lustre formation: ion-exchange of alkalies (Na and K) by Cu and Ag, diffusion of the metal ions into the glaze and reduction of the metal ions to metallic nanoparticles.[8]

Chemical mappings obtained directly on lustre decoration show a homogenous distribution of copper but an inhomogeneous distribution of silver. In Fig. 5, copper appears well distributed over all the lustre decoration but silver appears to form spots some several tens of microns in width, excluding in some cases the presence of copper. These silver spots are linked to blue spots seen on OM in reflectance mode. Also, an inverse correlation between the presence of copper and silver and alkalies such as sodium is seen. The copper and silver-rich areas corresponding to the lustre decoration lines are much less rich in sodium than the glaze.

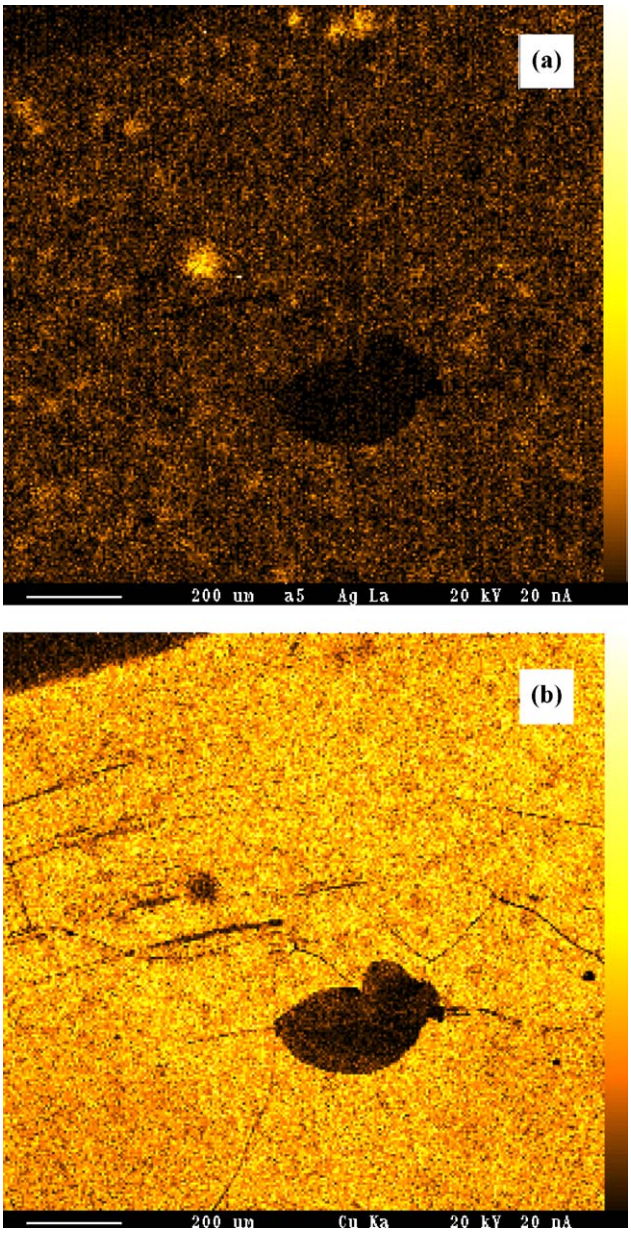

Fig. 5. Chemical maps obtained by means of EMPA on a 1 mm × 1 mm area on the surface of sample R4. (a) Accordingly to OM images an inhomogeneous distribution of silver forming scattered silver-rich spots on the lustre decoration surface can be seen. (b) Homogenous distribution of copper on the lustre decoration surface. From these maps, the silver-rich spots seem to exclude the presence of copper.

3.3. Copper nanoparticles development inside the glass matrix

The TEM images in Fig. 6 show that nanoparticles vary in size and amount during the lustre formation process from sample R1 to R4. In sample R1, small nanoparticles of about 10 nm mean diameter scattered throughout in the glass matrix can be observed. Surprisingly, nanoparticles appear deep inside into the glaze, 200 nm below the glaze surface. In sample R2, nanoparticles appear to form a discontinuous layer parallel to the glaze surface and two populations of nanoparticles can be distinguished according to their size: nanoparticles with a mean diameter about 10 nm and nanoparticles with a mean diameter around 20 nm. The bigger nanoparticles appeared in the first 100 nm depth into the glaze, and the smaller occur from 100 nm up to 200 nm in depth. In sample R3, a higher density of nanoparticles appears when compared to the previous samples, forming a continuous layer parallel to the glaze surface and in a range of mean diameters from 10 to 20 nm. The bigger nanoparticles appear in the first 100 nm depth into the glaze while the smaller ones appeared from 100 nm up to 200 nm depths. In sample R4, only one population of nanoparticles with a mean diameter of 20 nm appeared parallel to the glaze surface, forming a continuous layer at 100 nm depth into the glaze. EELS spectra acquired on three nanoparticles on sample R4 confirmed that they are mainly copper as shown in Fig. 7.

It is worth noticing that while observing the samples through TEM, the glass matrix suffered alteration due to the interaction of the electron beam with the sample, resulting in a granular texture which should not be confused with the nanoparticles forming the lustre metal-glass nanocomposite.

Low irradiation angle diffraction patterns were acquired in order to determine the main crystalline phases present. The only crystalline phases determined are metallic copper and silver as seen in Fig. 8 and listed on Table 4. The lustre formation process gives no crystalline phase initially in sample R1, metallic copper appears on sample R2, R3 and R4, and small amounts of metallic silver in sample R3 and R4.

SR-XRD diffraction patterns obtained in transmission geometry revealed not only copper but also cassiterite (SnO_2) allocated in-depth the glaze near to the main ceramic body as seen In Fig. 9 and listed in Table 5. Metallic copper showed evolution of the 1 1 1 diffraction line of metallic copper through samples R2, R3 and R4 as seen In Fig. 10. The intensity of the 1 1 1 Cu reflection increases and narrows in width from sample R2 to sample R4, in agreement with the increase in the amount and size of copper nanocrystals observed in the TEM images (see Fig. 1 and Table 2). In order to estimate the mean diameter of copper nanocrystals, the diffraction line profile was Gaussian fitted and the mean sizes of the copper particles calculated from the full width at half maximum applying the Scherrer equation. The mean nanocrystal diameter for sample R2 is around 9.28 nm, for sample R3 the mean is close to sample R2 with values around 9.14 nm, but for sample R4 the mean nanocrystal diameter increases to 21.95 nm. The results are summarized in Table 2. These data confirm an increase in the average size of the copper nanoparticles only from sample R3 to R4, in agreement with the sizes observed at TEM. No metallic copper 1 1 1 reflection appears in sample R1.

4. Discussion and interpretation of the measurements

Chemical analyses during the lustre formation process indicate that the incorporation of copper and silver in the lustre layer is linked to a decrease in the alkalies (Na and K) from the glaze as seen on Table 1. Metallic copper is the main crystalline phase present in the lustre reproductions; however, metallic silver has been detected by means of low angle XRD as seen in

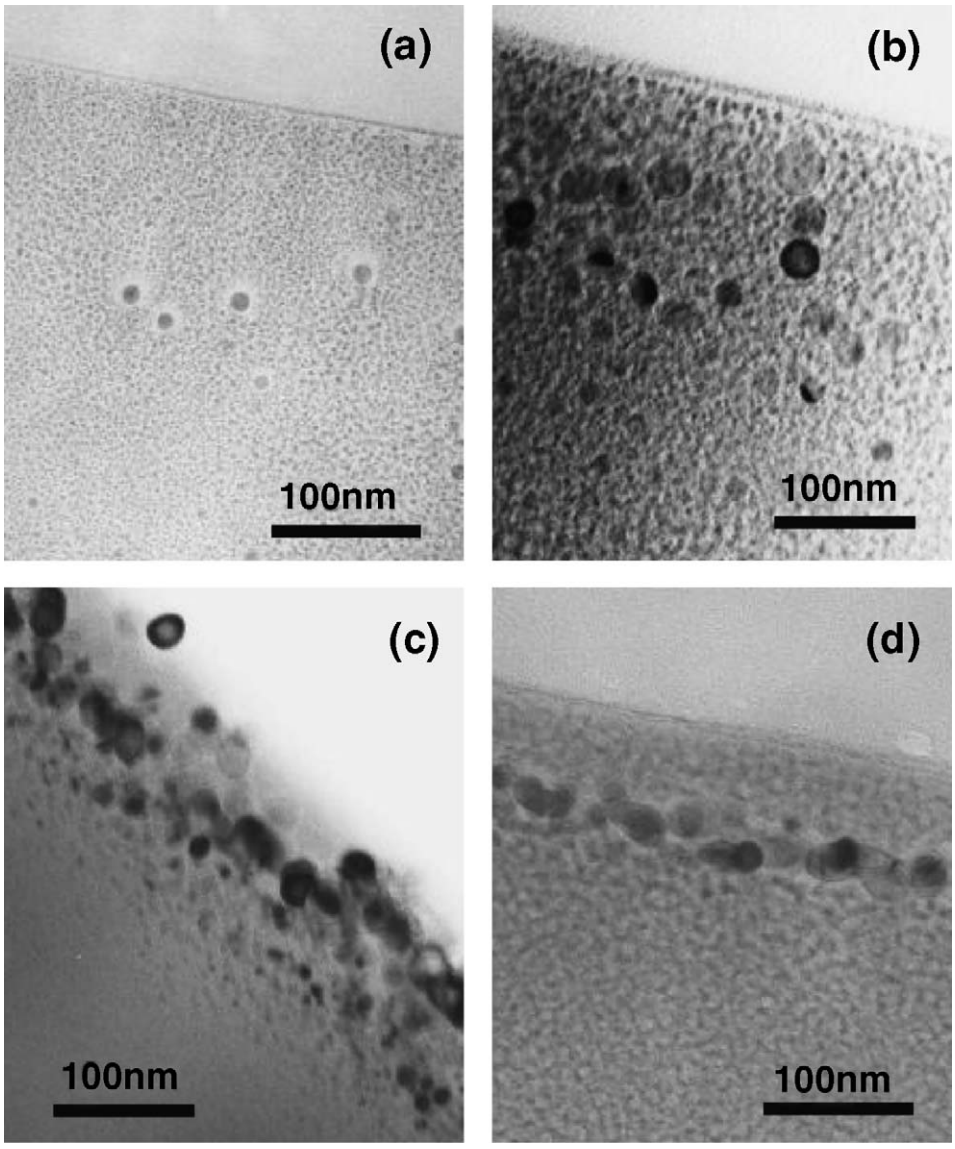

Fig. 6. TEM images obtained during the copper nanocrystallization process inside the glass matrix. (a) Sample R1 small nanoparticles about 10 nm mean diameter appear scattered in the glass matrix. (b) Sample R2, two populations of copper nanoparticles of 10 and 20 nm mean diameter appear forming a discontinuous layer parallel to the glaze surface. (c) Sample R3, two populations of copper nanoparticles of 10 and 20 nm mean diameter appear forming a continuous layer parallel to the glaze surface. (d) Sample R4, a continuous almost monolayer of copper nanoparticles with a mean diameter of 20 nm appears parallel to the glaze surface.

Figs. 8 and 10. Metallic silver nanocrystals are heterogeneously distributed in clusters in the lustre decoration, and as SR-XRD in transmission geometry provides low statistics on the surface, it is difficult to get any signal from the silver nanocrystals present in the glaze.

Metallic copper nanocrystals increase in amount through samples R1, R2, R3 and R4 according to the 1 1 1 reflection intensity, but only in size for sample R4 as seen in Fig. 3 and Table 2. For samples R1, R2 and R3, the lustre nanostructure exhibits nanocrystal size dependence on the depth, suggesting that a Cu^+ gradient exists inside the bulk glaze as seen in Fig. 6. This gradient can be explained as a result of the ion-exchange process. Close to the glass surface, the ionic-exchange process has been more intense, there is a higher Cu^+ concentration, and copper nanocrystals can grow easily up to 20 nm, but deeper into the glaze, where the ion-exchange process is less intense the concentration of Cu^+ is less, copper nanocrystals do not grow so easily and only nanocrystals around 10 nm in diameter are present. However, in sample R4, only nanocrystals with a mean diameter of 20 nm appear close to the glass surface. The disappearance of smaller nanocrystals in sample R4 could be due to a ripening process as in a closed system where the mass of the crystals is conserved (Oswald ripening). It would imply that in sample R4, the ion-exchange process has been exhausted at the outermost part of the glaze and then, some of the smaller crystalline phases dissolve to supply material to other crystals of the same phase that are growing. Thus, in sample R4, small metallic copper nanocrystals, less stable than bigger nanocrystals, have been redissolved to coarser the bigger nanocrystals which are close to the glass surface.

Reflecting OM as seen in Fig. 2, indicates that the lustre appears scattered at first, forming small spots linked to copper

Table 4
Spacing list from the crystalline phases present in the glazes and obtained from DRX data in reflection geometry and transmission geometry

DRX technique	Sample	*d* (Å) (measured)	*d* (Å) (JCPDF)	*h k l*	Phase
Low irradiation angle at 1.5418 Å in reflection geometry	R1	–	–	–	–
	R2	2.08	2.08	1 1 1	CuM
	R3	2.37	2.36	1 1 1	AgM
		2.08	2.08	1 1 1	CuM
		1.80	1.81	2 0 0	CuM
		1.27	1.28	2 2 0	CuM
	R4	2.37	2.36	1 1 1	AgM
		2.08	2.08	1 1 1	CuM
		1.80	1.81	2 0 0	CuM
		1.27	1.28	2 2 0	CuM
SRS Station 9.6 at 0.866 Å in transmission geometry	R1	3.32	3.35	1 1 0	SnO_2
		2.65	2.64	1 0 1	SnO_2
		2.38	2.37	2 0 0	SnO_2
		1.74	1.76	2 1 1	SnO_2
	R2	3.32	3.35	1 1 0	SnO_2
		2.65	2.64	1 0 1	SnO_2
		2.38	2.37	2 0 0	SnO_2
		2.09	2.08	1 1 1	CuM
		1.74	1.76	2 1 1	SnO_2
	R3	3.32	3.35	1 1 0	SnO_2
		2.65	2.64	1 0 1	SnO_2
		2.38	2.37	2 0 0	SnO_2
		2.09	2.08	1 1 1	CuM
		1.74	1.76	2 1 1	SnO_2
	R4	3.32	3.35	1 1 0	SnO_2
		2.65	2.64	1 0 1	SnO_2
		2.38	2.37	2 0 0	SnO_2
		2.09	2.08	1 1 1	CuM
		1.74	1.76	2 1 1	SnO_2

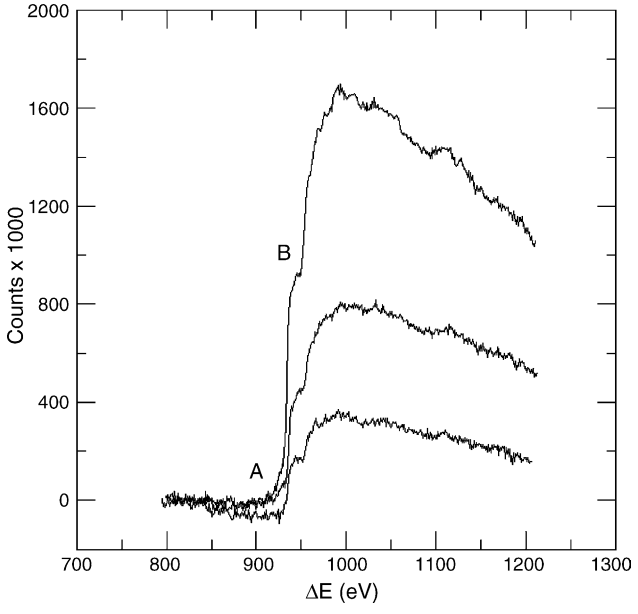

Fig. 7. Characteristic metallic copper EELS spectra obtained on three different nanocrystals from sample R4. The three spectra show the absorption edges (A) Cu L3 at 931 eV and (B) Cu L2 at 951 eV characteristics of copper.

nanoparticles agglomerates which increase in density and join together until they occupy the whole surface. These areas are orange or yellow depending of the spot size, and the metallic shine is first achieved at the edges of the lustre decorations and is linked to the presence of more yellow spots. Some blue and purple spots appear in samples R3 and R4 corresponding to clusters of metal silver particles according to Figs. 2 and 5. The final, almost homogeneous orange-yellow surface containing some blue spots of silver fits with OM observations of medieval lustres.[1,4]

Reflectance and absorbance spectra (Figs. 3 and 4) obtained from these samples confirm that lustre optical properties such as

Table 5
Crystalline phases list obtained from DRX data in reflection geometry and in transimission geometry from lustre glazes

DRX technique	Phase	JCPDF file
Low irradiation angle at 1.5418 Å in reflection geometry	AgM	2-1098
	CuM	89-2838
SRS Station 9.6 at 0.866 Å in transmission geometry	SnO_2	41-1445
	CuM	89-2838

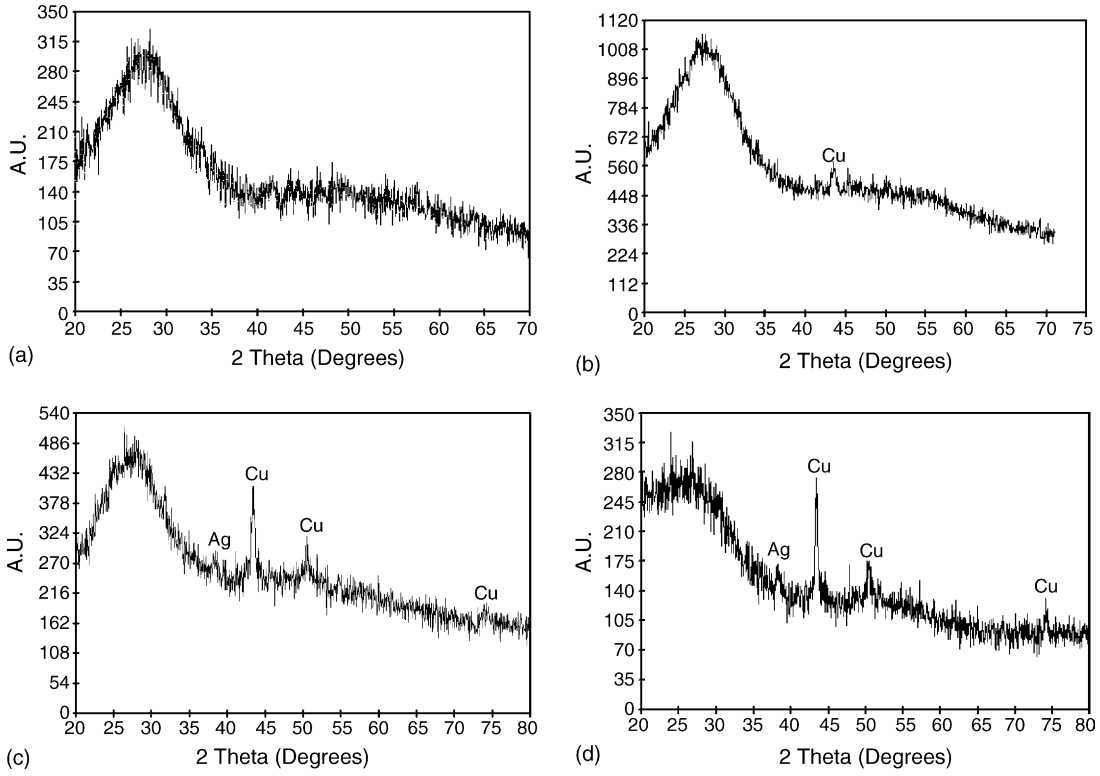

Fig. 8. Low angle XRD pattern acquired on lustre reproductions surfaces. (a) Sample R1, no crystalline phases are present; (b) sample R2, only metallic copper appears; (c) sample R3 and (d) sample R4, metallic copper and silver are detected.

absorption, reflectance and thus colour, strongly depend on the dipole plasmon resonance of the metallic copper and silver particles present in the lustre layer. The dipole plasmon resonance occurs when metallic nanoparticles are irradiated by light, then the oscillating electric field causes the conduction electrons to oscillate coherently displacing the electron cloud from to the nuclei. The absorption produced by the collective oscillation of the electrons is known as the dipole plasmon resonance of the particle, which for spherical copper nanoparticles is expected to be at 560 nm and for silver nanoparticles is at 430 nm.[19,20]

However, there are complicating factors in understanding optical properties of the nanoparticles appearing in lustre decorations, e.g. as particles maybe are close enough together to give electromagnetic coupling, and/or the supporting substrate may change the spectra expected.[21–23]

The copper nanoparticles in lustre decoration increase in number from sample R2 to sample R4, reducing the intercrystalline distances, thus resulting in changes in the plasmon peak position and width as a consequence of dipole interactions among the nanoparticles. In sample R2, there is a large interparticle distance, the particles “perceive” little change in the environment and there is no dipole coupling, while in samples R3 and R4, the interparticle distances are smaller and the dipole plasmon resonance absorption band changes showing a red shift and an absorption increase in the red region seen in Fig. 4 as in Thearith et al.[23] It is interesting to note that the mean nanopar-

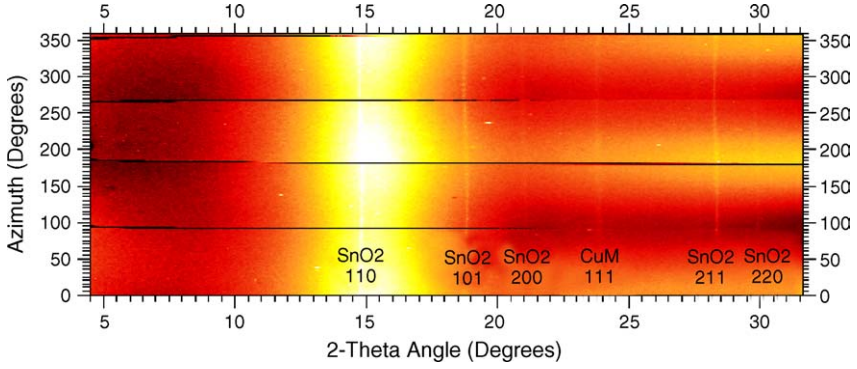

Fig. 9. SR-DRX at 0.866 Å wavelength azimuth transform pattern from sample R4, with clear bump at low angle associated to amorphous glass and cassiterite (SnO_2) and metallic copper (CuM) as the main crystalline phases present. CuM 1 1 1 reflection is wide giving and indirect evidence of its nanometric size. Cassiterite has been detected only in transmission geometry because is only present in-depth the glaze, near to the main ceramic body in low amounts, acting as opacifier.

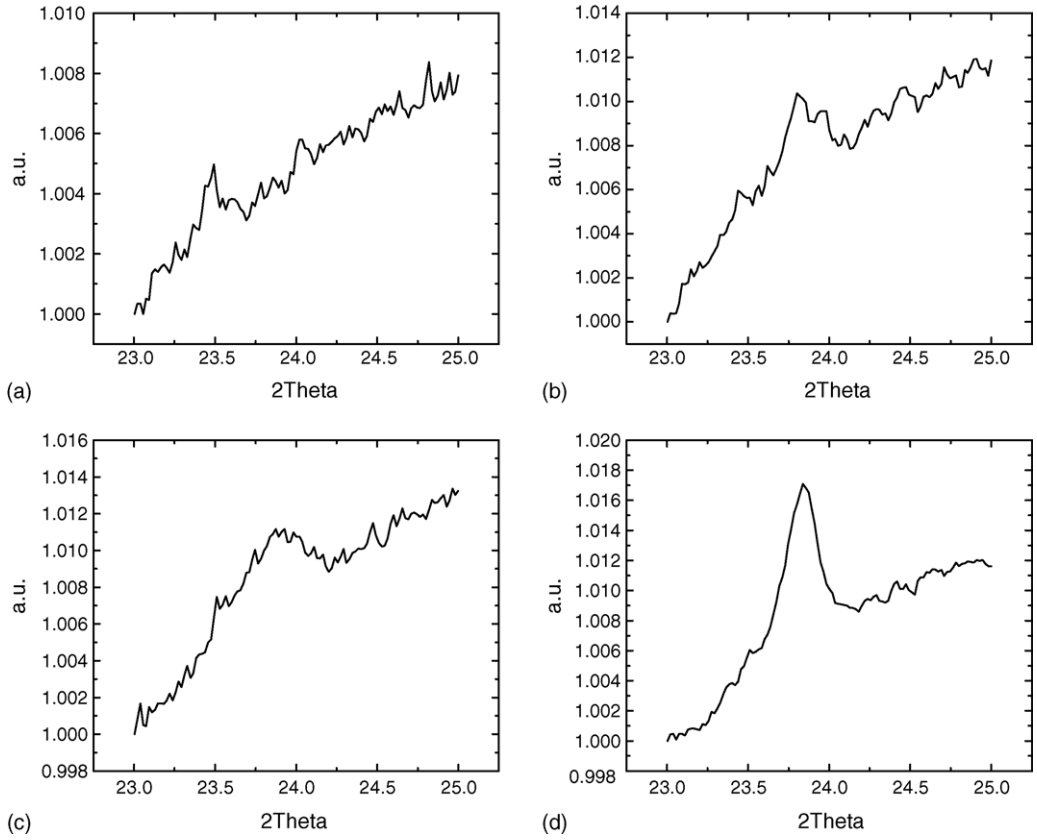

Fig. 10. SR-DRX at 0.866 Å wavelength patterns showing the evolution of the 1 1 1 Cu reflection. It increases in height and becomes narrower according to an increase in the number and size of copper nanocrystals. (a) The 1 1 1 Cu reflection in sample R1, (b) the 1 1 1 Cu reflection in sample R2, (c) the 1 1 1 Cu reflection in sample R3, (d) the 1 1 1 Cu reflection in sample R4.

ticles diameter in sample R2 is the same as in sample R3 as seen in Fig. 10 and Table 2, supporting the hypothesis that the interparticle distance is the main parameter which governs the plasmon redshift, and the increase of the absorption in the red region in lustre decorations.

During the development of the lustre, the layer of nanocrystals progressively conceals the underlying lead glaze increasing its RSCE in the red region and enhancing the RSC as seen in Fig. 3. The RSCE is almost the same through all samples except for sample R1 which corresponds to the lead glaze with practically no influence from the nanocrystals. The RSC is strongly enhanced in samples R3 and R4, which seems to be a consequence of the change of the refractive index of the glaze due to metallic copper nanocrystals and dipole coupling in the lustre nanostructure, giving it its characteristic gloss, that is to say, the reflectance of the fully developed lustre surface.

The silver dipole plasmon absorption band appears concealed by the strong absorption in the blue region of the supporting substrate (the glaze) and cannot be observed in either the absorption or the RSCE spectra. However, in the RSC spectra, a blue reflection appears, as a consequence of a strong absorption around 430 nm linked to the dipole plasmon resonance of silver nanocrystals, as seen on Fig. 3. This discrepancy can be explained by means of the concealing effect of the bulk lead glaze by the lustre layer. The silver dipole plasmon absorption band expected around 430 nm appears concealed by the absorption in the blue region of the supporting substrate and cannot be seen in the absorption or the RSCE spectra. However, once the lustre layer is fully developed, the incident light does not penetrate into the lead glaze and the effect of the blue absorption in very low, while the reflectance in the blue due to the silver plasmon becomes more prominent. In these conditions, the RSC spectrum corresponds to the light reflected directly from the glaze surface and thus not affected by the absorbing effects of the bulk glaze.

Hence, the colour of the glaze surface is affected by the presence of copper and silver nanoparticles and differs when calculated from the RSCE or RSC. The colour of the glaze surface calculated from the RSCE spectra listed in Table 1 shows a strong dependence on the presence of copper nanocrystals in the lead glazes. In sample R1 (λ_D 475 nm 0.07%), almost no nanocrystals are present, and the glaze has a bluish colour corresponding to the lead glaze. However, samples R2 (λ_D 583 nm 0.1%), R3 (λ_D 582 nm 0.14%) and R4 (λ_D 585 nm 0.19%) have a colour corresponding to yellowish-orange thus concealing the original lead glaze colour. It is also seen in Fig. 6 that the reduction of the copper interparticle distance through these samples seems to be responsible for an increase in the RSCE colour excitation purity from 0.1% in R2, to 0.14% in R3 and 0.19% in sample R4.

The colour of the glaze surface calculated from the RSC spectra appears to be affected not only by copper but also by

silver nanocrystals. According to Fig. 6 and Table 1 when the copper interparticle distances are reduced calculated λ_D from RSC is shifted towards reddish values; in samples R1 (λ_D 582 0.21%) and R2 (λ_D 586 nm 0.15%) with a colour corresponding to yellowish-orange, sample R3 (λ_D 589 nm 0.65%) with a colour corresponding to orange, while in sample R4 (λ_D 602 nm 0.32%), the colour corresponds to reddish-orange. However, the specular reflectance in some parts of lustre decorations appears purple. Observation of the specular reflectance through a reflecting microscope confirms the presence of blue spots that EPMA mappings demonstrated that correspond to silver clusters as seen in Figs. 2 and 5. Thus, the blue and red reflectance component seen in Fig. 3 corresponds to silver and copper nanoparticles, respectively, and the resulting mixture of blue plus red is interpretated by the eye as purple.

It is worth noticing that TEM-EELS measurements alter the glass matrix resulting to a granular texture which is not directly related to the copper nanocrystallization process in lustre formation as seen in Fig. 6. This alteration may have occurred because of the interaction of the TEM electron beam with the sample which produces a reducing effect on the major constituent chemical species present in the glass matrix.

5. Conclusions

Lustre nanostructure shows crystal size dependence as a function of depth, supporting the proposition that Cu^+ and Ag^+ ions from the raw paint applied on the surface are exchanged with Na^+ and K^+ from the glaze, followed by the crystallization of metallic copper nanocrystals inside the glass matrix.

During the lustre formation, the centre of mass of the Cu nanoparticles has a tendency to shift toward the surface accompanied by the disappearance of the smaller nanocrystals, resulting from a pronounced coarsening of the nanoparticles and causing a reduction of the interparticle distances. Thus, the dipole plasmon coupling between copper nanoparticles appears and it seems to be responsible for the lustre shine and colour.

Nevertheless, the colour from the glaze surface differs when calculated from diffuse or specularly reflected light. Diffuse coloration appears strongly affected by copper nanocrystals, which are the most abundant, while specular coloration is not only affected by copper but also by the presence of an inhomogeneous distribution of silver nanocrystals. The effect of the silver nanocrystals in diffuse light is concealed by the bulk glaze, but in specular reflectance silver nanocrystals are responsible for the characteristic lustre blue reflectance giving a purplish colour when combined with reddish emission of copper.

The close agreement between TEM-EELS and SR-XRD results suggests that the point information obtained by TEM-EELS agrees with the averaged information obtained by SR-XRD.

Acknowledgements

The research presented in this paper has been funded by the project BQU 2002-03162 of the Spanish Ministry of Science and by a project of the Comunidad de Trabajo de los Pirineos (CTP/DAER 03007514), through which the collaboration between researchers of the CEMES Toulouse and the University of Barcelona has been possible. The authors would also like to thank Mr. Alejandro Barberà, a potter still working in lustre, for his help and facilities in traditional firing. Also, thanks are due to Dr. Josefina Pérez-Arantegui of the Universidad de Zaragoza, Dr. Isabel Pastoriza of the Universidad de Vigo and Dr. Triniat Pradell of the Universitat Politècnica de Catalunya for fruitful discussions. We are grateful to Anne-Sophie Ramm from CEMES Toulouse for her help and guidance in the TEM sample preparations. The SR data were collected at Daresbury Laboratory during a visit in the framework of the Memorandum of Understanding signed between CCLRC and UB/UPC.

References

1. Pérez-Arantegui, J., Molera, J., Larrea, A., Pradell, T., Vendrell-Saz, M., Borgia, I., Brunetti, B. G., Cariati, F., Fermo, P., Mellini, M., Sgamellotti, A. and Viti, C., *J. Am. Ceram. Soc.*, 2001, **84**, 442–446.
2. Pérez-Arantegui, J. and Larrea, A., *Trends Anal. Chem.*, 2003, **22**(5), 327–329.
3. Padeletti, G. and Fermo, P., *Appl. Phys.*, 2003, **A76**, 515–525.
4. Roqué, J., Pradell, T., Molera, J. and Vendrell-Saz, M., *J. Non-Cryst. Solids*, 2005, **351**, 568–572.
5. Perez-Arantegui, J., Larrea, A., Molera, J., Pradell, T. and Vendrell-Saz, M., *Appl. Phys.*, 2004, **A79**, 235–239.
6. Caigher-Smith, A., *Lustre Pottery: Technique, Tradition and Innovation in Islam and the Western World*. Faber & Faber, London, UK, 1985.
7. Pérez Camps, J., La Cerámica de Reflejo Metálico en Manises 1850–1960. Catálogo de la Exposición. Colección Ethnos, València, Spain, 1998.
8. Molera, J., Mesquida, M., Pradell, T., Pérez-Arantegui, J. and Vendrell-Saz, M., *Archaeometry*, 2001, **43**, 455–460.
9. Pradell, T., Molera, J., Vendrell-Saz, M., Pérez-Arantegui, J., Pantos, E., Roberts, M. and DiMichiel, M., *J. Am. Ceram. Soc.*, 2004, **87**, 1018–1023.
10. Pradell, T., Molera, J., Roqué, J., Smith, A. D., Crespo, D., Pantos, E. and Vendrell-Saz, M., *J. Am. Ceram. Soc.*, 2005, **88**, 1281–1289.
11. Smith, A. D., Pradell, T., Molera, J., Vendrell, M., Marcus, M. A. and Pantos, E., *J. Phys. France IV*, 2003, **104**, 519–522.
12. Kenneth, J. K., *Nanoscale Materials in Chemistry*. Wiley-Interscience, New York, 2001.
13. Bobin, O., Schvoerer, M., Miane, J. L. and Fabre, J. F., *J. Non-Cryst. Solids*, 2003, **332**, 28–34.
14. Padovani, S., Borgia, I., Brunetti, B., Sgamellotti, A., Giulvi, A., D'Acapito, F., Mazzoldi, P., Sada, C. and Battaglin, G., *Appl. Phys. A*, 2004, **79**(2), 229–233.
15. Kanaya, K. and Okayama, S. J., *Phys. D: Appl. Phys.*, 1972, **5**, 43–58.
16. Hammersley, A. P., Svensson, O., Hanfland, M., Fitch, A. N. and Hausermann, D., *High Press. Res.*, 1996, **14**, 235–248.
17. Vendrell-Saz, M., Molera, J. and Tite, S., *Archaeometry*, 2000, **42**, 325–340.
18. Magruder III, R. H., Weeks, R. A., Zuhr, R. A. and Whichard, G., *J. Non-Cryst. Solids*, 1991, **129**, 46–53.
19. Bohren, Craig F. and Huffman, Donald R., *Absorption and Scattering of Light by Small Particles*. Wiley-Interscience, New York, 1998.
20. Salzemann, C., Lermé, J., Urban, J. and Lisiecki, I., *Chem. Mater.*, 2005, **17**, 1279–1283.
21. Maxwell Garnett, J. C., *Phil. Mag.*, 1904, **CCIII**, 385–420.
22. Lance Kelly, K., Coronado, E., Zhao, L. L. and Shatz, G. C., *J. Phys. Chem. B*, 2003, **107**, 668–677.
23. Thearith, U., Liz-Marzán, L. M. and Mulvaney, P., *J. Phys. Chem. B*, 2001, **105**, 3441–3452.